THE JOURNAL OF BIOLOGICAL CHEMISTRY VOL. 289, NO. 32, pp. 22365–22376, August 8, 2014

Type II Fatty Acid Synthesis Is Essential for the Replication of *Chlamydia trachomatis*[*]

Received for publication, May 23, 2014, and in revised form, June 13, 2014 Published, JBC Papers in Press, June 23, 2014, DOI 10.1074/jbc.M114.584185

Jiangwei Yao[‡], Yasser M. Abdelrahman[§¶], Rosanna M. Robertson[‖], John V. Cox[§], Robert J. Belland[§], Stephen W. White[‖], and Charles O. Rock[‡1]

From the Departments of [‡]Infectious Diseases and [‖]Structural Biology, St. Jude Children's Research Hospital, Memphis, Tennessee 48105, the [§]Department of Microbiology, Immunology, and Biochemistry, University of Tennessee Health Science Center, Memphis, Tennessee 38163, and the [¶]Department of Microbiology and Immunology, Faculty of Pharmacy, Cairo University, Cairo 11562, Egypt

Background: *Chlamydia trachomatis* has a phospholipid composition that resembles its eukaryotic host, but it contains branched-chain fatty acids of chlamydial origin.
Results: The inhibition of the enoyl-acyl carrier protein reductase (FabI) in chlamydial fatty acid synthesis blocks *C. trachomatis* replication.
Conclusion: Bacterial FASII is required for *C. trachomatis* proliferation.
Significance: FabI is a therapeutic target against *C. trachomatis*.

The major phospholipid classes of the obligate intracellular bacterial parasite *Chlamydia trachomatis* are the same as its eukaryotic host except that they also contain chlamydia-made branched-chain fatty acids in the 2-position. Genomic analysis predicts that *C. trachomatis* is capable of type II fatty acid synthesis (FASII). AFN-1252 was deployed as a chemical tool to specifically inhibit the enoyl-acyl carrier protein reductase (FabI) of *C. trachomatis* to determine whether chlamydial FASII is essential for replication within the host. The *C. trachomatis* FabI (*Ct*FabI) is a homotetramer and exhibited typical FabI kinetics, and its expression complemented an *Escherichia coli fabI*(Ts) strain. AFN-1252 inhibited *Ct*FabI by binding to the FabI·NADH complex with an IC_{50} of 0.9 μM at saturating substrate concentration. The x-ray crystal structure of the *Ct*FabI·NADH·AFN-1252 ternary complex revealed the specific interactions between the drug, protein, and cofactor within the substrate binding site. AFN-1252 treatment of *C. trachomatis*-infected HeLa cells at any point in the infectious cycle caused a decrease in infectious titers that correlated with a decrease in branched-chain fatty acid biosynthesis. AFN-1252 treatment at the time of infection prevented the first cell division of *C. trachomatis*, although the cell morphology suggested differentiation into a metabolically active reticulate body. These results demonstrate that FASII activity is essential for *C. trachomatis* proliferation within its eukaryotic host and validate *Ct*FabI as a therapeutic target against *C. trachomatis*.

Chlamydia trachomatis is a Gram-negative, obligate intracellular bacterial parasite that causes a range of human diseases (1). *C. trachomatis* infections are the most prevalent bacterial sexually transmitted diseases, causing tens of millions of new cases a year, and the leading cause of infectious blindness affecting hundreds of millions of people. *C. trachomatis* has a dimorphic life cycle (2). The elementary body (EB)[2] is the metabolically quiescent, infectious, extracellular form that initiates the infection by attaching to a suitable eukaryotic host cell. Once internalized by the host cell, the EB differentiates into the metabolically active and noninfectious reticulate body (RB) that replicates inside of a vacuole called the chlamydial inclusion. At 16–20 h after the initial chlamydial infection, RBs start differentiating into EBs, and by 48–72 h after the infection, most RBs have converted into EBs. The lysis of the host cell releases the infectious EBs, and the cycle of infection continues.

The major *C. trachomatis* phospholipid classes are the same as those of the host cell, but they also contain branched-chained fatty acids made by *C. trachomatis* at the 2-position of some phospholipids (branched chains constitute ~20% of the total acyl chains in *C. trachomatis* phospholipids) (3). The branched-chain fatty acids are thought to be produced by chlamydial type II fatty acid synthesis (FASII), but it is unknown whether FASII is required for phospholipid acquisition/synthesis in *C. trachomatis*. The current model is that *C. trachomatis* acquires host phospholipids, a portion of which are subsequently deacylated at the 2-position and reacylated with endogenously made *anteiso*-15:0 (3). The host $cPLA_2$ has been implicated in the deacylation reaction because pharmacological inhibition of the Raf/MEK/ERK/$cPLA_2$ pathway decreases *C. trachomatis* titers (4). However, recent studies using $cPLA_2$ knockdown human

[*] This work was supported, in whole or in part, by National Institutes of Health Grants GM034496 (to C. O. R.), AI070693 (to R. J. B), and Cancer Center Support Grant CA21765. This work was also supported by the American Lebanese Syrian Associated Charities.

The atomic coordinates and structure factors (code 4Q9N) have been deposited in the Protein Data Bank (http://wwpdb.org/).

[1] To whom correspondence should be addressed: Dept. of Infectious Diseases, St. Jude Children's Research Hospital, 262 Danny Thomas Pl., Memphis, TN 38105. Tel.: 901-495-3491; Fax: 901-495-3099; E-mail: charles.rock@stjude.org.

[2] The abbreviations used are: EB, elementary body; ACP, acyl carrier protein; FabI, enoyl-ACP reductase; *Ct*FabI, enoyl-ACP reductase of *C. trachomatis*; *Sa*FabI, enoyl-ACP reductase of *S. aureus*; FASII, bacterial type II fatty acid synthesis; LOS, lipooligosacchride; RB, reticulate body; MOMP, chlamydial major outer membrane protein; BisTris, 2-[bis(2-hydroxyethyl)amino]-2-(hydroxymethyl)propane-1,3-diol.

cells found that a decrease in $cPLA_2$ activity has no effect on *C. trachomatis* growth (5). In mouse cells, $cPLA_2$ knockdown increases chlamydial titers, suggesting that $cPLA_2$ is more likely involved in intracellular immunity (5). One function of FASII is to generate the 3-hydroxy fatty acids for lipopolysaccharide synthesis in Gram-negative bacteria (6). The outer membrane of *C. trachomatis* is decorated with a similar lipooligosaccharide (LOS) that contains 18 and 20 carbon 3-hydroxy fatty acids (7–9). The inhibition of LOS biosynthesis in *C. trachomatis* does not block RB proliferation but does prevent the differentiation of RB into EB, resulting in the accumulation of noninfectious RBs within the chlamydial inclusion (10). Thus, one function of FASII would be to provide these 3-hydroxy fatty acids for LOS synthesis in *C. trachomatis*, but it is unknown whether FASII is needed for phospholipid synthesis.

We used AFN-1252 as a chemical biology tool to specifically inhibit the enoyl-acyl carrier protein (ACP) reductase (FabI) (11–13) and assess the role of FASII in *C. trachomatis* replication. *C. trachomatis* is predicted to encode a FASII system that depends on FabI (Fig. 1). AFN-1252 inhibits *C. trachomatis* FabI (*Ct*FabI) by forming a tight ternary *Ct*FabI·NADH·AFN-1252 complex visualized at 1.8 Å resolution. AFN-1252 treatment arrests the replication of *C. trachomatis* when added at any time during the infectious cycle, and when administered at the beginning of the infection, it blocks development at a single cell RB-like state. These data show that FASII is required for *C. trachomatis* replication and validate *Ct*FabI as a suitable target for antichlamydial therapy.

EXPERIMENTAL PROCEDURES

Molecular Biology—The *fabI* gene (CT104) of *C. trachomatis* strain D/UW-3/Cx (NCBI Microbial Genomes Database) was optimized for expression in *Escherichia coli* through GeneArt gene synthesis (Invitrogen). A NdeI cleavage site was engineered at the 5′-end of the gene with a start codon in the NdeI site, whereas a 6-histidine tag, stop codon, and a EcoRI cleavage site were sequentially engineered at the 3′-end of the gene. The *fabI* sequence was cloned into the plasmids pET21a (Novagen) and pPJ131, pBluescript plasmid (Stratagene) with a modified multiple cloning site (14), via the NdeI and EcoRI (New England Biolabs) cloning sites. The pET21a-*CtfabI* expression plasmid was transformed in BL21 Tuner cells (Novagen) for protein expression and purification.

The pPJ131-*CtfabI* plasmid was transformed into the *fabI* temperature-sensitive *E. coli* strain JP1111 to determine complementation. The JP1111 strain is viable at 30 °C but nonviable at 42 °C without *fabI* gene complementation. The JP1111 cells were transformed with the pPJ131-*CtfabI* plasmid, the pPJ131 parent plasmid, and pBluescript plasmids expressing *fabI* from *E. coli* and *Bacillus anthracis* and then plated on Luria-Bertani (LB) plates at 30 °C with 100 μg/ml carbenicillin. The transformed cells were restreaked onto LB plates with 100 μg/ml carbenicillin and grown at 30 or 42 °C to determine whether the *C. trachomatis fabI* complements the *E. coli fabI* activity.

CtFabI Expression and Purification—BL21 Tuner cells harboring the pET21a-*CtfabI* plasmid were grown in LB medium with 100 μg/ml carbenicillin at 37 °C and 225 rpm shaking until A_{600} reached 0.6–0.8. The culture was then induced with 1 mM isopropyl 1-thio-β-D-galactopyranoside and grown at 17 °C and 225 rpm shaking overnight. Cells were pelleted and washed twice with 20 mM Tris, pH 8.0, and finally resuspended in 20 mM Tris, pH 8.0 (40 ml/liter of culture). Cells were lysed via a cell disruptor, and the C-terminal 6-histidine-tagged *Ct*FabI was purified via nickel chelation chromatography. Briefly, the cell lysate was centrifuged at 20,000 × *g* to remove the cell debris. The resulting supernatant was poured over a nickel-nitrilotriacetic acid resin column (4 ml of resin/liter of cell culture) to bind the protein to the column. The column was washed with 5 column volumes of 20 mM Tris, pH 8.0, and 20 mM imidazole, followed by 5 column volumes of 20 mM Tris, pH 8.0, 500 mM NaCl, and 50 mM imidazole. The protein was eluted from the column with 20 mM Tris pH 8.0 and 250 mM imidazole. The fractions containing protein, as determined by the Bradford reagent, were collected and dialyzed against 20 mM Tris, pH 8.0, 10 mM EDTA, and 150 mM NaCl at 4 °C overnight. A pure protein (>95%) running at ~32 kDa (theoretical average mass of 32,783.49 with N-terminal methionine) was observed on a NuPAGE 10% BisTris gel. Over 25 mg of purified *Ct*FabI was obtained per liter of culture.

Analytical Ultracentrifugation—Analytical ultracentrifugation experiments and analysis were carried out as described previously by the St. Jude Molecular Interaction Analysis Facility (15, 16). Experiments were performed in 20 mM Tris, pH 7.5, 10 mM EDTA, 150 mM NaCl buffer. Chlamydial FabI has a calculated molecular mass of 32,783 Da.

Enzymology—FabI activity was determined by monitoring the optical density at 340 nm to measure the conversion of NAD(P)H to $NAD(P)^+$. The enzyme reactions were 100 μl in volume and were performed and monitored in Costar UV half-area 96-well plates with a SpectraMax 340 instrument taking 340-nm readings at 10-s intervals at 30 °C. The substrate NADH and NADPH were obtained from Sigma-Aldrich. The substrate crotonyl-ACP from *S. aureus* was synthesized as described previously (17). For velocity measurements, the *Ct*FabI enzyme was added to 100 μM crotonyl-ACP and a 250 μM concentration of either NADPH or NADH in 20 mM Tris, pH 8.0. Upon finding that *Ct*FabI prefers NADH over NADPH by over 1000-fold, NADH was used for future measurements. For determination of K_m of crotonyl-ACP, 100 nM *Ct*FabI was added to 200 μM NADH and 3, 6, 12, 24, 36, or 48 μM crotonyl-ACP. For determination of K_m of NADH, 100 nM *Ct*FabI was added to 50 μM crotonyl-ACP and 5, 10, 15, 20, 30, 50, and 75 μM NADH. The reaction was mixed for 10 s by the mix function on the plate reader, and data were acquired at 10-s intervals for 5 min. The initial velocity was calculated from the linear phase of the progress curve, and the initial velocity data were fit using a standard Michaelis-Menten equation to determine the apparent K_m. The IC_{50} of AFN-1252 and triclosan against *Ct*FabI was measured as above at saturating substrate concentrations (50 μM crotonyl-ACP and 200 μM NADH) against different concentrations of AFN-1252 and triclosan (0, 0.156, 0.312, 0.625, 1.25, 2.5, 5, and 10 μM). All kinetic experiments were run in triplicate.

Protein Thermal Shift Analysis—Protein thermal shift analysis was conducted to determine the mode of binding of AFN-1252 to *Ct*FabI. Solutions (30 μl) of *Ct*FabI (10 μM), *Ct*FabI (10

μM) + AFN-1252 (10 μM), *Ct*FabI (10 μM) + NADH (100 μM), *Ct*FabI (10 μM) + NADH (100 μM) + AFN-1252 (10 μM), *Ct*FabI (10 μM) + NAD^+ (100 μM), and *Ct*FabI (10 μM) + NAD^+ (100 μM) + AFN-1252 (10 μM) in a final buffer of 100 μM Tris, pH 7.0, 0.5% DMSO, and 2.5× Sypro Orange Dye (Sigma-Aldrich) were added to wells of ThermoGrid optically clear PCR plates (Denville Scientific). The plates were centrifuged for 5 min at 1000 × *g* to remove air bubbles and then subjected to thermal shift analysis in the ABI 7300 real-time PCR system. The temperature was ramped from 25 to 95 °C at 1 °C/min with the fluorescence read six times at each temperature ramp. The resulting data were fit to a Boltzmann sigmoidal equation to determine the melting point of the *Ct*FabI under each particular ligand combination. Each ligand condition was replicated six times, and each replicate was subjected to independent analysis to determine the thermal melting point. The melting points of the six independent runs per ligand condition were averaged to determine the thermal melting point for each ligand condition. Representative thermal shift runs along with the average thermal melting points are presented.

Crystallization and Structure Determination—The *Ct*FabI protein was incubated for 1 h with 0.4 mM NADH and 0.25 mM AFN-1252 at 2 mg/ml and then concentrated to 7 mg/ml for crystallization. Initial trials were performed at 18 °C against the PEGs Suite and PEGs II Suite (Qiagen), and several conditions produced small crystals that were subsequently optimized. Crystals suitable for x-ray analysis were eventually obtained in 28% (w/v) polyethylene glycol 300, 0.1 M HEPES (pH 7.5), and 0.2 M potassium formate. Crystals were flash-frozen directly from mother liquor in liquid nitrogen and diffracted to 1.8 Å in space group P43 with unit cell dimensions $a = 96.2$ Å, $b = 96.2$ Å, $c = 263.0$ Å. Diffraction data were collected at the SER-CAT beam line ID22 at the Advanced Photon Source and processed using HKL2000 (18). The *Ct*FabI structure was solved by maximum likelihood molecular replacement using the program Phaser (19) and the coordinates of apo-FabI from *Brassica napus* (Protein Data Bank accession code 1ENO) as the search model. The structure was completed by iterative rounds of refinement using Phenix (20) and manual rebuilding using Coot (21). The refinement was monitored by following the R_{free} value calculated from a random subset (5%) of omitted reflections. A summary of the data reduction and structure refinement statistics is provided in Table 1, and the coordinates have been deposited in the Protein Data Bank (accession code 4Q9N). The images of the protein structure were generated with PyMOL (22).

C. trachomatis Strains and Propagation—*C. trachomatis* serovar L2 (strain 434/Bu) was used for most experiments. *C. trachomatis* was propagated by standard infection through centrifugation protocols in HeLa cells grown in DMEM containing 10% fetal bovine serum (23). Cell cultures were grown in Costar 6-well cell culture plates (Corning) with 3 ml of medium. Depending on the specific experimental conditions, AFN-1252 was added either immediately postinfection or some number of hours postinfection. Infected cells were harvested at 48 h postinfection, and the number of infectious units was determined through reinfection. Serovar D was propagated similarly but harvested 72 h after infection.

Genome Copy Number Quantitation—HeLa 229 cells were infected with *C. trachomatis* 434/Bu (NCBI Reference Sequence: NC_010287.1) at a multiplicity of infection of 1 in 6-well plates. DNA was collected at 0, 7, 14, 27, and 53 h postinfection. For some samples, AFN-1252 was added at the time of infection at a concentration of 10 μM. Nucleic acid was collected using MasterPure (Epicenter), and samples were processed according to the manufacturer's instructions. After RNA was removed by digestion with RNase A, the DNA was repurified by isopropyl alcohol precipitation. DNA quantification was carried out using a LightCycler 480 system (Roche Applied Science). A standard curve was generated using purified chromosomal template DNA at concentrations ranging from 10 to 0.001 ng/well, and samples (2 ng/well) were then analyzed in triplicate according to the manufacturer's instructions. The gene for 16 S RNA was selected for quantification, and primer design and Roche Universal probe library selection were carried out using Web-based ProbeFinder software version 2.50 (Roche Applied Science). Forward and reverse Primer sequences were 5′-GAGATGGAGCAAATCCTCAAA and 5′-ACTTCATGTAGTCGAGTTGCAGA, respectively. Data analysis and standard curve construction were carried out using LightCycler 480 software. Measurements were made in triplicate.

Localization Analyses—Mouse monoclonal antibodies directed against chlamydial Hsp60 were provided by Dr. R. P. Morrison, and antibodies against the chlamydial major outer membrane protein (MOMP) were obtained from Meridian Life Sciences. AlexaFluor-conjugated secondary antibodies and Hoechst were obtained from Invitrogen. HeLa cells infected with *C. trachomatis* serovar D or *C. trachomatis* serovar L2 in the absence or presence of AFN-1252 were fixed at 48 h postinfection by incubation in 4% paraformaldehyde in phosphate-buffered saline (PBS) for 10 min. Following rinsing in PBS, the cells were permeabilized by incubation in methanol for 10 s and rinsed again in PBS. The cells were then incubated with monoclonal antibodies directed against chlamydial Hsp60 followed by secondary antibodies conjugated to AlexaFluor 488 prior to analysis on a Zeiss Axioplan 2 epifluorescent microscope. In some cases, cells were double-stained with antibodies directed against MOMP and Hsp60.

C. trachomatis Metabolic Labeling—Labeling experiments were performed on *C. trachomatis* cultures 20 h postinfection. Experiments were conducted in Costar 6-well cell culture plates with 3 ml of medium in each well. Radiolabeled chemicals were from American Radiolabeled Chemicals. For [U-^{14}C]isoleucine labeling experiments, the cell culture was washed with 1 ml of PBS and then incubated in 3 ml of fresh DMEM with 10% FBS. For [U-^{14}C]glucose labeling experiments, the cell culture was washed with 1 ml of PBS and then incubated in 3 ml of fresh DMEM with 10% FBS containing only 0.45 g/liter glucose to increase the specific activity of the labeled glucose added later. AFN-1252 was added to the culture for 30 min before the radioactive labels (10 μCi of either [U-^{14}C]isoleucine or [U-^{14}C]glucose) were added. DMSO (equal volume to AFN-1252 additions) was added to the infected culture for 30 min for the no drug controls. Labeling was allowed for 4 h at 37 °C and 5% CO_2 before cells were harvested and extracted for

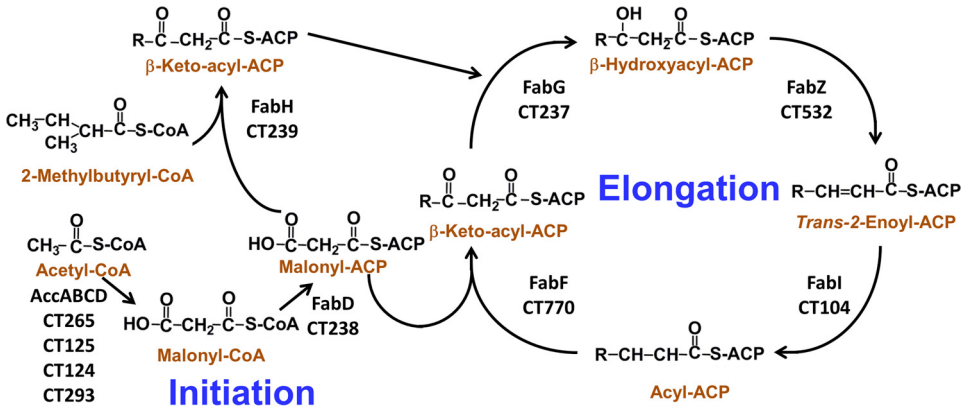

FIGURE 1. **Fatty acid synthesis in *C. trachomatis*.** *C. trachomatis* encode the genes for FASII. The locus tags of these genes in strain D/UW-3/Cx are annotated *below* the enzyme names. Acetyl-CoA is converted into malonyl-CoA by the acetyl-CoA carboxylase enzyme complex (*AccABCD*). Malonyl-CoA is then converted into malonyl-ACP by the enzyme malonyl-CoA-ACP transacylase (*FabD*). Fatty acid synthesis is initiated by 3-oxoacyl-ACP synthase III (*FabH*) condensing malonyl-ACP with either acetyl-CoA for straight-chain fatty acid synthesis or 2-methylbutyryl-CoA for *anteiso* branched-chain fatty acid synthesis. The resulting 3-ketoacyl-ACP is reduced by 3-oxoacyl-ACP reductase (*FabG*), and the resulting 3-hydroxyacyl-ACP is dehydrated by 3-hydroxyacyl-ACP dehydratase (*FabZ*) into *trans-2*-enoyl-ACP. The last step in the cycle is the conversion of *trans-2*-enoyl-ACP to acyl-ACP by FabI. Known genes for making unsaturated fatty acids are absent in *C. trachomatis*. Long-chain acyl-ACP is used for phospholipid synthesis, and long-chain 3-hydroxyacyl-ACP is used for LOS synthesis.

lipids via the Bligh and Dyer protocol (24). Radioactive incorporation was measured by counting the lipid extracts on an LS6500 multipurpose scintillation counter. Measurements were made in triplicates, and the averages with S.E. were reported. For the HeLa cell controls, a mock infection (same infection protocol with no *C. trachomatis*) was performed on the cells, and the same labeling procedure was performed. Cell viability was measured with the NucleoCounter (New Brunswick Scientific) following the manufacturer's protocol.

RESULTS

C. trachomatis FASII—A bioinformatics analysis of the *C. trachomatis* genome suggests that it encodes a complete FASII (Fig. 1). Branched-chain fatty acids arise from the utilization of 2-methylbutyryl-CoA by FabH to prime FASII (25). 2-Methylbutyryl-CoA is generated from isoleucine by the branched-chain α-ketoacid dehydrogenase complex. The structure and mechanism of the branched-chain α-ketoacid dehydrogenase complex is similar to the pyruvate dehydrogenase complex. The genes encoding both the branched-chain α-ketoacid dehydrogenase complex (CT340, CT400, and CT557) and the pyruvate dehydrogenase complex (CT245 to -247) were identified in the *C. trachomatis* genome. This bioinformatics analysis predicts that *C. trachomatis* has the gene set for the synthesis of branched-chain and hydroxy fatty acids that cannot be obtained from the host. Branched-chain fatty acids are incorporated into chlamydial phospholipids (26), and the straight-chain 3-hydroxy fatty acids are found in the LOS of this organism (27–29). The gene(s) for unsaturated fatty acid synthesis are absent.

CtFabI Is an Enoyl-ACP Reductase—The enoyl-ACP reductase plays a determinant role in establishing the rate of FASII (30, 31). The predicted FabI sequences from different chlamydial strains have greater than 99% amino acid identity and are homologous to the *Sa*FabI (31% identity, 49% similarity). The function of *Ct*FabI in FASII was assessed by determining whether *Ct*FabI expression complemented the growth phenotype of an *E. coli fabI*(Ts) mutant. The *E. coli* codon-optimized

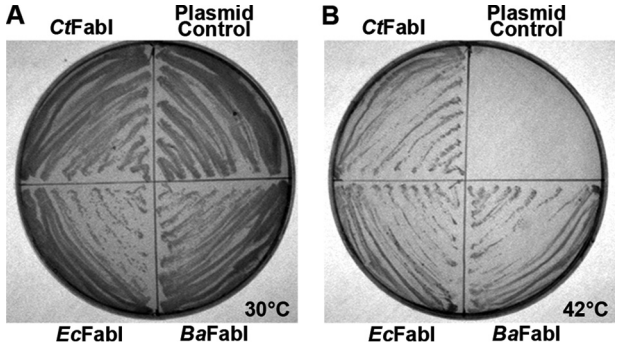

FIGURE 2. **The CT104 gene functions as a FabI.** *A*, growth of the temperature-sensitive *E. coli* strain JP1111 (*fabI*(Ts)) transformed with plasmids expressing either the *C. trachomatis*, *E. coli* (*EcFabI*), or *B. anthracis* FabI (*BaFabI*) or the empty vector control under the permissive growth condition (30 °C). *B. anthracis* was used as a control to illustrate that a FabI from an organism that makes branched-chain fatty acids can complement the *E. coli* enzyme. *B*, growth of the same strain series at the non-permissive temperature (42 °C). Complementation of the growth phenotype at 42 °C indicates the expression of a functional enoyl-ACP reductase.

fabI gene from *C. trachomatis* D/UW-3/Cx was cloned into the pBluescript expression vector and transformed into *E. coli* strain JP1111 (*fabI*(Ts)) (32). At the permissive temperature (30 °C), strain JP1111 and all its transformants exhibited robust growth (Fig. 2*A*). At the non-permissive temperature (42 °C), strain JP1111 was unable to grow without a complementing *fabI* gene being present in the plasmid (Fig. 2*B*). The *E. coli*, *B. anthracis*, and *C. trachomatis fabI* genes all complemented growth at the non-permissive temperature, confirming that the *C. trachomatis fabI* gene product functioned as an enoyl-ACP reductase in the heterologous *E. coli* FASII.

*Ct*FabI was expressed, and the protein was purified by affinity chromatography (Fig. 3*A*). *Ct*FabI sedimented as a 128-kDa complex in analytical centrifugation experiments (Fig. 3*B*), which was consistent with *Ct*FabI as a homotetramer (131 kDa expected), like other characterized FabI proteins (33). The enzymatic reaction of *Ct*FabI was assessed by measuring NADH/NADPH conversion to $NAD^+/NADP^+$ at 340 nm. The *Ct*FabI catalyzed the turnover of NADH (K_m = 22.93 ± 3.16 μM) (Fig. 3*C*) into NAD^+ in the presence of crotonyl-ACP

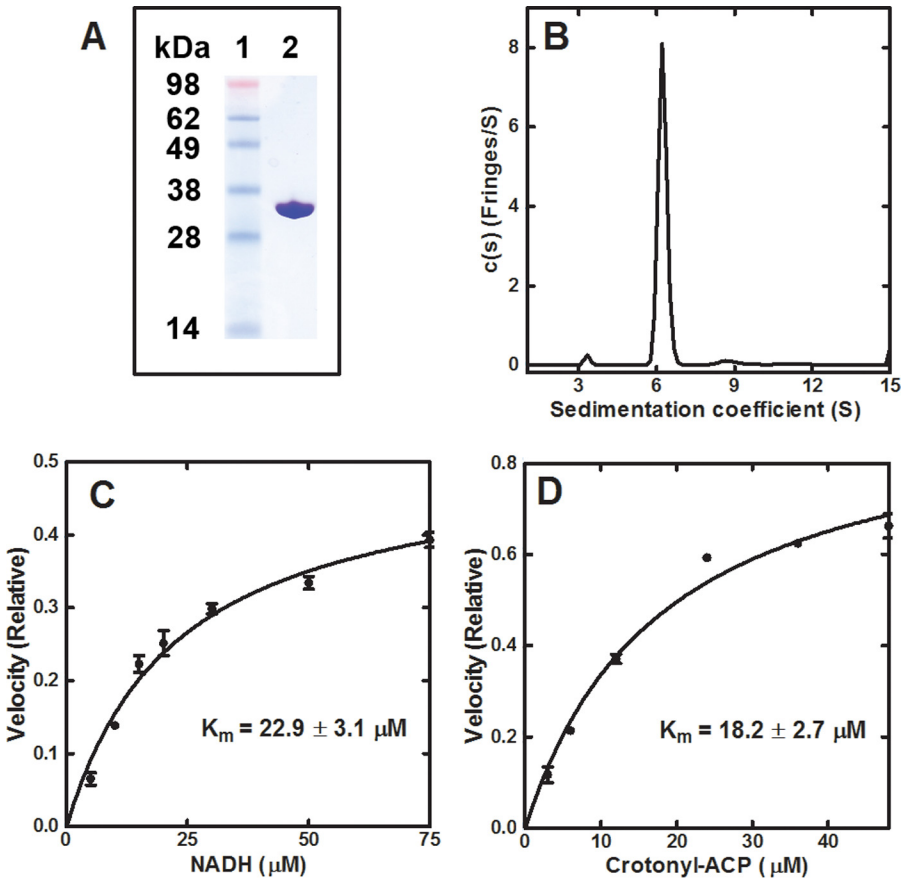

FIGURE 3. **Purification and biochemistry of *Ct*FabI.** *A*, *Ct*FabI was purified by affinity and gel filtration chromatography. Gel electrophoresis shows the purity of *Ct*FabI. *Lane 1*, standards; *lane 2*, *Ct*FabI (32.7 kDa). *B*, the sedimentation velocity profiles (fringe displacement) were fitted to a continuous sedimentation coefficient distribution model *c*(*s*). *Ct*FabI sedimented as a 128-kDa tetramer (131 kDa theoretical mass). *C*, initial velocities were determined in triplicate as a function of NADH concentration. *D*, initial velocities were determined in triplicate as a function of crotonyl-ACP concentration. The data points were fit to the Michaelis-Menten nonlinear regression fit in GraphPad Prism version 5. The fitted line is shown on the graph. The fitted K_m values with the S.E. values (*error bars*) are reported.

(K_m = 18.18 ± 2.67 μM) (Fig. 3*D*). NADPH was >1000-fold less efficient than NADH in supporting the reaction, consistent with *Ct*FabI preferring NADH like most bacterial FabIs, with the sole exception of *Sa*FabI (30, 34). The k_{cat} of *Ct*FabI with NADH and crotonyl-ACP was 15.6 ± 0.05 min^{-1}, which is similar in velocity to other characterized FabI enzymes (35). These biochemical experiments confirmed that *Ct*FabI was an enoyl-ACP reductase.

AFN-1252 Inhibition of CtFabI—The chemical biology approach was validated by determining the affinity and the mode of inhibition of AFN-1252 for *Ct*FabI. AFN-1252 exhibited an IC_{50} of 0.95 ± 0.21 μM against *Ct*FabI at saturating substrate concentrations (Fig. 4*A*). The IC_{50} against the prototypical FabI inhibitor, triclosan, was also determined (0.32 ± 0.08 μM). AFN-1252 inhibited *Sa*FabI by forming a FabI·NADPH·AFN-1252 complex (12, 17). The formation of this ternary complex on *Ct*FabI was demonstrated by examining the effects of AFN-1252 on the *Ct*FabI melting temperature using a protein thermal denaturation assay (Fig. 4*B*). *Ct*FabI had a melting temperature of 48 °C in the absence of any ligand. The addition of AFN-1252 did not shift the melting temperature, indicating the absence of a *Ct*FabI·AFN-1252 complex. The addition of NADH stabilized *Ct*FabI, as indicated by a shift in the melting temperature to 50.2 °C. The addition of NADH and AFN-1252 increased stability substantially by shifting the melting temperature to 65.8 °C. The addition of NAD^+ or NAD^+ and AFN-1252 to *Ct*FabI did not significantly increase the thermal stability, indicating the absence of a *Ct*FabI·NAD^+·AFN-1252 complex. These data indicated that AFN-1252 inhibited *Ct*FabI by binding to the *Ct*FabI·NADH complex. Thus, AFN-1252 is a sharp tool to study the effects of FASII inhibition on *C. trachomatis* replication in light of its selectivity, its binding affinity, and the absence of off-target effects on human cells (11, 36).

The FabI·NADH·AFN-1252 Ternary Complex—A 1.8 Å crystal structure of the ternary complex was solved to validate the biochemical characterization (Table 1). There were eight molecules of the ternary complex in the crystal asymmetric unit that represented two copies of the biological tetramer. The protomers were all structurally similar with a root mean square deviation between all main chain atoms of 0.17 Å. The electron densities of the co-factor NADH and the small molecule inhibitor in each of the eight active sites were well resolved. The comparison of the overall fold of *Ct*FabI with that of *Sa*FabI shows that both proteins have a seven-stranded parallel β-sheet flanked by 11 α-helices and several loops that are typical for FabIs (Fig. 5) (33). The active site contains the signature catalytic tyrosine and lysine residues (Tyr-188 and Lys-195) directly

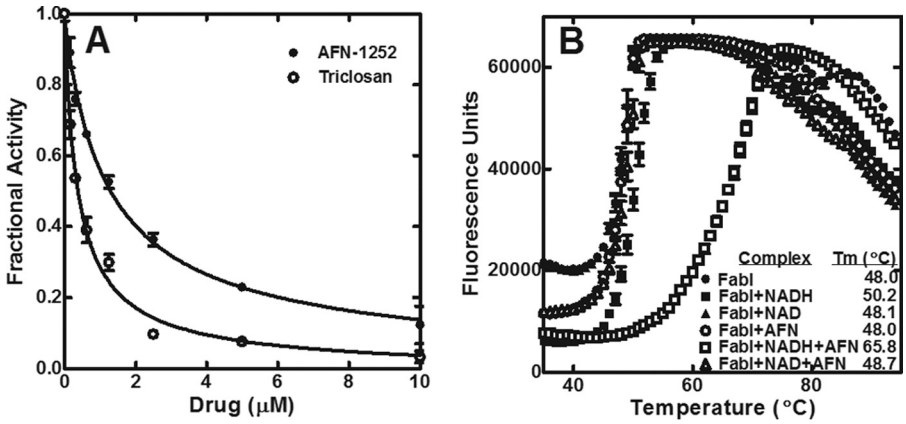

FIGURE 4. **AFN-1252 inhibition of *Ct*FabI.** *A*, initial velocities were determined in triplicate as a function of AFN-1252 (●) or triclosan (○) concentration. The data points were fit to the IC_{50} equation of the form, $v_i/v_0 = 1/(1 + [I]/IC_{50})$), using custom equation fit in GraphPad Prism 5. The fitted line is shown on the graph. The fitted IC_{50} values and S.E. values (*error bars*) are reported. *B*, protein thermal denaturation analysis was used to determine the melting point of FabI alone (●), FabI + NADH (■), FabI + NAD^+ (▲), FabI + AFN-1252 (○), FabI + NADH + AFN-1252 (□), and FabI + NAD^+ + AFN-1252 (△).

TABLE 1

X-ray crystallographic data and refinement statistics for *Ct*FabI·NADH·AFN1252 complex (Protein Data Bank entry 4Q9N)

Crystal	*Ct*FabI·NADH· AFN-1252
Data collection	
Space group	P43
Wavelength (Å)	1.0
Unit cell dimensions	
a (Å)	96.15
b (Å)	96.15
c (Å)	263.08
α, β, γ (degrees)	90, 90, 90
Molecules/ASU[a]	8
Resolution (Å) [b]	1.8 (1.85–1.80)[d]
Completeness (%)[b]	98.8 (95.1)
Redundancy[b]	6.3 (3.4)
No. of total reflections	335,128
No. of unique reflections	221,426
I/σ^b	15.5 (1.57)
R_{sym} [b,c]	12.2 (61.6)
Refinement statistics	
Resolution (Å)	1.8
No. of reflections	218,306
R_{work}/R_{free} (%)[d,e]	0.1863/0.2292
No. of atoms	19,232
Protein	17,700
Ligand/ion	576
Water	956
B-Factors (Å^2)	
Protein	25.4
Ligand/ion	22.7
Water	28.2
Root mean square deviations	
Bond length (Å)	0.006
Bond angle (degrees)	1.057
Ramachandran analysis	
Most favored (%)	97.5
Allowed (%)	3.3
Disallowed (%)	0.2

[a] Asymmetric unit.
[b] Values in parentheses are for the highest resolution shell.
[c] $R_{sym} = \Sigma|I - \langle I\rangle|/\Sigma\langle I\rangle$, where *I* is the observed intensity, and $\langle I\rangle$ is the average intensity of multiple observations of symmetry-related reflections.
[d] $r = \Sigma_{hkl}||F_o| - |F_c||/\Sigma_{hkl}|F_o|$.
[e] R_{free} is calculated from 5% of the reflections excluded from refinement.

adjacent to the bound cofactor (33). *Ct*FabI has two additional loops comprising residues 56–69 and 84–104, but they are located at the surface and do not impact the conserved FabI fold or the active site (Fig. 5). AFN-1252 consists of oxotetrahydronaphthyridine and 3-methylbenzofuran groups linked by a *cis*-amide. The carbonyl oxygen atom of the *cis*-amide makes hydrogen bond interactions with the 2′-hydroxyl of the nicotinamide ribose and the hydroxyl of Tyr-188, whereas the pyridyl nitrogen and the *N*-acyl hydrogen of the oxotetrahydronaphthyridine moiety make hydrogen bonds with the peptide backbone carbonyl and amide of Ser-130, respectively (Fig. 6*A*). The 3-methylbenzofuran group forms an edge-to-face π-interaction with the side chain of Phe-235. FabI is characterized by a flexible substrate-binding loop, called the "flipping loop," that "closes" to orient the substrate with respect to the cofactor nicotinamide ring for reduction (37–39). This loop (residues 228–240) adopts the "closed" conformation that has been observed with other FabI·inhibitor complexes (12, 40, 41), and the *cis*-amide stacks onto the nicotinamide ring to apparently mimic the targeted double bond of the bound substrate (33).

The *Ct*FabI and *Sa*FabI (Protein Data Bank accession code 4FS3) structures are very similar, with a root mean square deviation on main chain atoms of 1.4 Å, and the modes of binding of the cofactor and inhibitor are practically identical (Fig. 6). One difference is that Phe-204 on the *Sa*FabI substrate-binding loop (residues 195–207) is replaced by Ile-236 in *Ct*FabI; however, the adjacent Phe-235 of *Ct*FabI remains positioned to make the edge-to-face π-interaction with the 3-methylbenzofuran group of the inhibitor. FabI proteins have a relatively unconserved and conformationally flexible substrate-binding α-helical loop that creates a "lid" over the active site following the binding of the cofactor and substrate (17, 40). In *Sa*FabI, Met-99 within this segment (residues 97–102) extends into the active site pocket toward the oxotetrahydronaphthyridine group of AFN-1252, and this key hydrophobic interaction is critical for the high-affinity binding of AFN-1252 to *Sa*FabI (Fig. 6*B*) (17). Comparison of the *Ct*FabI and *Sa*FabI structures revealed not only that *Ct*FabI contains a two-residue deletion, including this methionine, but that the loop (residues 130–133) was apparently more flexible and lacked the ordered α-helical segment found in *Sa*FabI (Fig. 6). Most significantly, the loop is flipped away from the inhibitor-binding site and, as a result, no residues of *Ct*FabI are positioned to replace the lost hydrophobic interaction. In addition, the movement of this loop reduces the binding surface of AFN-1252 such that the oxotetranapthyridine moiety occupies a solvent-exposed cavity (Fig. 6*A*). In comparison, the lid

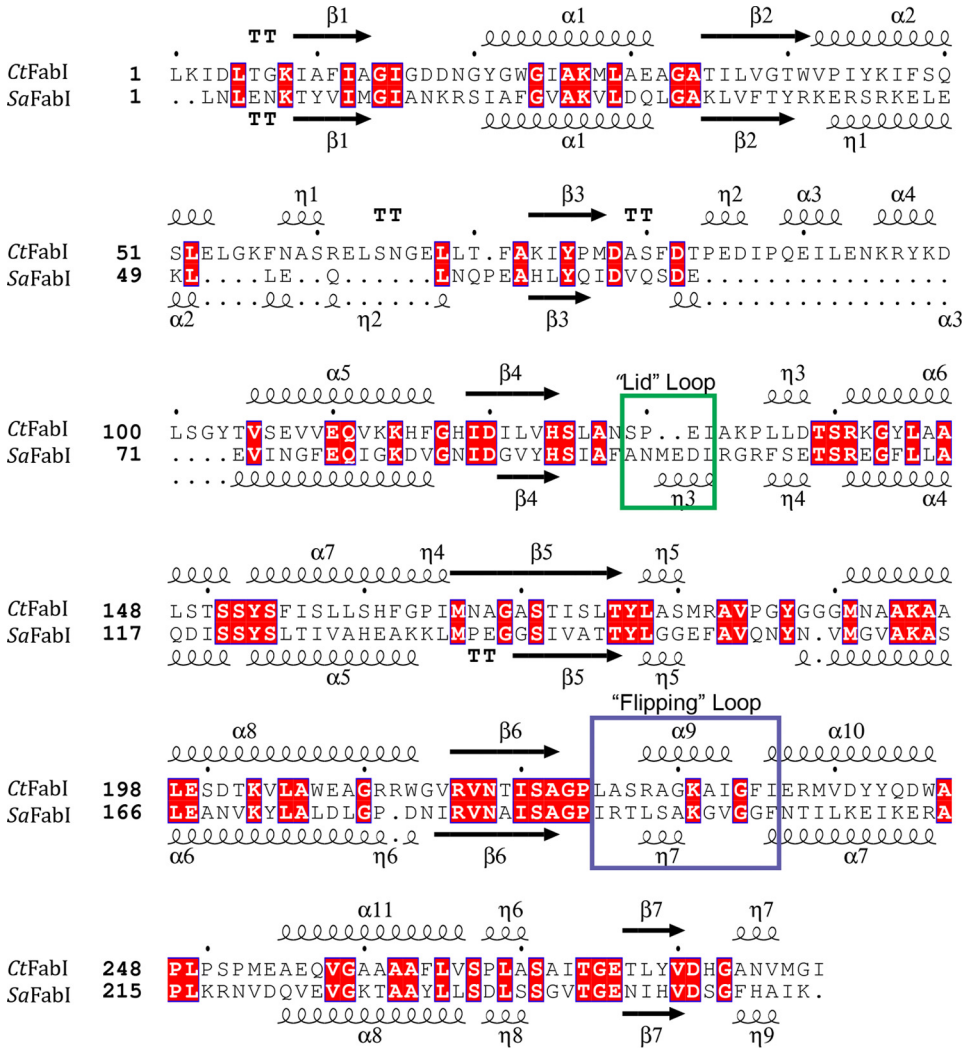

FIGURE 5. **Comparison of the primary and secondary structures of *Ct*FabI and *Sa*FabI.** The primary and overall secondary structures of *Ct*FabI and *Sa*FabI are conserved. The two substrate binding loop regions are surrounded by *boxes* with *colors* corresponding to the structural elements depicted in Fig. 6. Notably, the helical loop η3 in *Sa*FabI that contains the critical Met-99 residue is replaced in *Ct*FabI with a less structured loop region containing a two-residue deletion. *Red*, identical residues. Structure-based sequence alignments were performed using Salign (47) and analyzed using ESPript3 (48).

adopts a more tightly closed conformation around the inhibitor in the *Sa*FabI structure (Fig. 6*B*). These differences provide a structural explanation for why AFN-1252 exhibits lower affinity against *Ct*FabI compared with *Sa*FabI. However, the key interactions between AFN-1252 and the peptide backbone and cofactor are maintained in the *Ct*FabI·NADH·AFN-1252 complex, offering opportunities for the structure-based design of modified AFN-1252 derivatives that can exploit the larger substrate pocket in *Ct*FabI.

AFN-1252 Inhibits Fatty Acid Synthesis—The effect of AFN-1252 on branched-chain fatty acid synthesis was determined to verify that the drug blocked bacterial FASII. The branched-chain fatty acids are synthesized by initiating FASII with a short-chain branched-chain acyl-CoA, followed by five rounds of elongation using malonyl-ACP derived from acetyl-CoA (Fig. 1) (25). Straight-chain fatty acids are built from acetyl-CoA molecules entirely (25, 42). Isoleucine is the precursor to 2-methylbutyryl-CoA via the bacterially encoded branched-chain α-ketoacid dehydrogenase, whereas glucose is a precursor to acetyl-CoA in both mammalian and bacterial metabolic schemes. Incorporation of the radioactivity from [U-^{14}C]glucose into the lipid fraction indicated total fatty acid synthesis activity in both the host and the parasite. Because the eukaryotic host cannot make branched-chain fatty acids, incorporation of radioactive [U-^{14}C]isoleucine into the lipid fraction primarily reflected the FASII activity of *C. trachomatis*. One caveat was that isoleucine is broken down into acetyl-CoA by the mammalian host (43), which can then be incorporated into fatty acids derived from both host and parasite. Therefore, we also measured the amount of [U-^{14}C]isoleucine incorporated into uninfected HeLa cells to serve as an estimate for the extent of this metabolic conversion.

Cell viability and [U-^{14}C]glucose and [U-^{14}C]isoleucine incorporation into the uninfected HeLa cells when treated with 50 μM of AFN-1252 were determined to ensure that AFN-1252 does not exhibit off-target effects on the host cell. Treatment of the host cell with 50 μM AFN-1252 did not affect radioactive incorporation from [U-^{14}C]glucose (Fig. 7*A*) or cell viability (>95%). Infected HeLa cells were pulse-labeled for 4 h with [U-^{14}C]glucose 20 h following the initial infection to measure

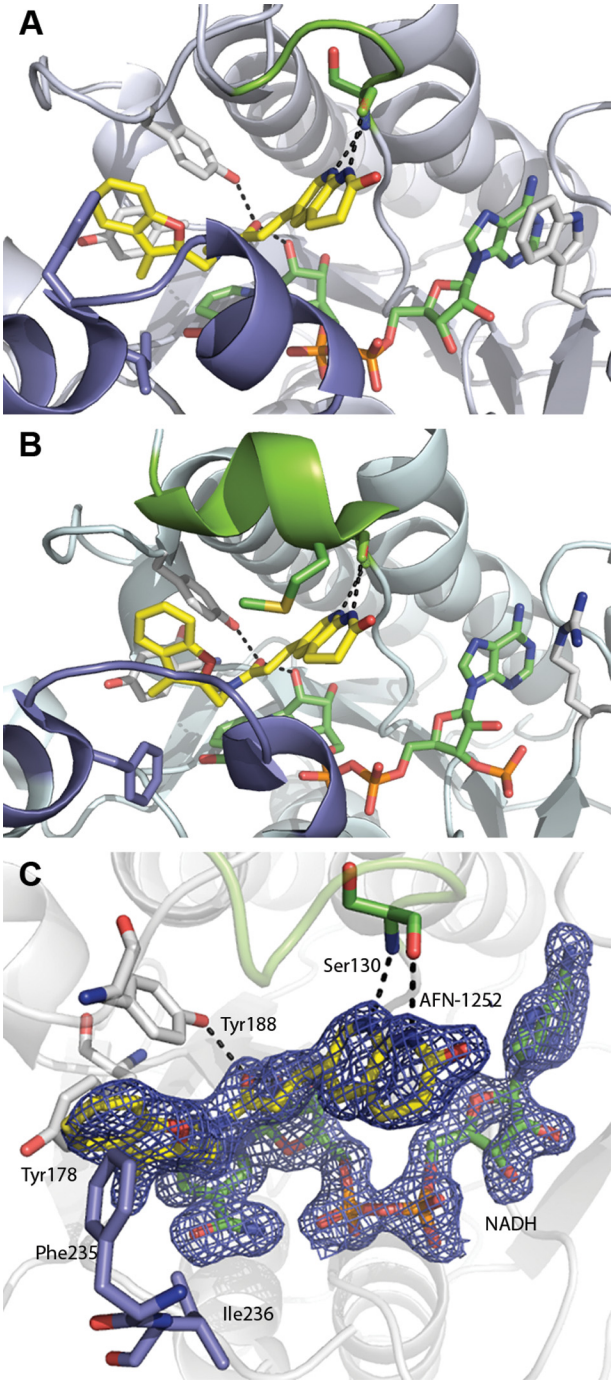

FIGURE 6. **FabI·NADH·AFN ternary complex structure.** *A*, *Ct*FabI·NADH·AFN-152 ternary complex (Protein Data Bank accession code 4Q9N). *B*, *Sa*FabI·NADPH·AFN-1252 ternary complex (Protein Data Bank accession code 4FS3). The *color schemes* are the same in *A* and *B*. AFN-1252 is shown in *yellow*, and NADPH/NADH is shown in *green*. The flexible, substrate-binding flipping loop is *colored slate*, and the poorly conserved lid loop is *colored chartreuse*. *Black dashes* show the conserved hydrogen bonding network for AFN-1252. In *Sa*FabI, the substrate lid adopts a more ordered, helical structure and orients Met-99 into the active site toward the inhibitor. In contrast, in *Ct*FabI, the active site is more open, due to the less structured conformation of the lid. *C*, active site of the *Ct*FabI·NADH·AFN-1252 ternary complex. AFN-1252 binds within a hydrophobic pocket composed of Tyr-178, Phe-235, and Ile-236, with Phe-235 positioned for π-interactions with the 3-methylbenzofuran of AFN-1252. The 2′-hydroxyl of NADH and the hydroxyl of Tyr-188 make hydrogen bonds with the carbonyl of the linking *cis*-amide, and the Ser-130 peptide backbone carbonyl and amide make hydrogen bonds with the pyridyl nitrogen and the *N*-acyl hydrogen of the oxotetrahydronaphthyridine of AFN-1252. σA-weighted $2F_o - F_c$ electron density is shown for AFN-1252 and NADH contoured at 1.5 σ.

the effect of AFN-1252 on the total fatty acid biosynthetic activity in the infection model. The infected cell population incorporated 7.5 times more radioactivity compared with uninfected HeLa cells (Fig. 7*A*). AFN-1252 treatment reduced [U-^{14}C]glucose incorporation by over 70% compared with the untreated infected cells. Similar labeling experiments with [U-^{14}C]isoleucine revealed that infected HeLa cells incorporated over 6 times more radioactivity into the lipid fraction than did uninfected HeLa cells, consistent with an increased synthesis of branched-chain fatty acids in the infected cells (Fig. 7*B*). AFN-1252 treatment of infected HeLa cells caused a dose-dependent decrease in [U-^{14}C]isoleucine incorporation (Fig. 7*C*). In cells treated with 50 μM AFN-1252, [U-^{14}C]isoleucine incorporation was the same as in uninfected cells (Fig. 7, *B* and *C*), demonstrating that AFN-1252 blocked the increase in [U-^{14}C]isoleucine incorporation resulting from the infection. The incorporation of [U-^{14}C]isoleucine into uninfected cells and the residual incorporation in AFN-1252-treated cells were attributed to the conversion of isoleucine to acetyl-CoA (43), which was used for host fatty acid synthesis. These results demonstrated that AFN-1252 inhibited *C. trachomatis* fatty acid synthesis in the infection model.

AFN-1252 Inhibits C. trachomatis Replication—The role of endogenous fatty acid synthesis in regulating *C. trachomatis* growth was determined by treating the *Chlamydia*-HeLa cell infection model with AFN-1252. HeLa cells infected with *C. trachomatis* serovar L2 were incubated with increasing concentrations of AFN-1252 for 48 h. The number of inclusions in an infected monolayer (Fig. 8*A*) and the number of infectious units (EBs) formed (Fig. 8*B*) were both decreased in a dose-dependent manner by AFN-1252. At >6 μM AFN-1252, no infectious particles were generated. AFN-1252 effectively decreased the infectious titers when added as late as 32 h postinfection, consistent with a critical role for FASII throughout the entire developmental cycle (Fig. 8*C*). The number of chlamydial genomes per cell decreased over time when infected cells were treated with 10 μM AFN-1252, suggesting that AFN-1252 arrested the replication of *C. trachomatis*, and the host cell cleared the organisms that had been internalized (Fig. 8*D*).

The stage in the developmental cycle where AFN-1252 arrested chlamydial growth was determined by double-staining individual cells with a mouse monoclonal antibody directed against chlamydial Hsp60 (cytoplasmic marker, *green*) and Hoechst (*blue*) to mark host cell nuclei. AFN-1252 treatment caused a dose-dependent decrease in the size of the chlamydial inclusion in HeLa cells infected with *C. trachomatis* serovar L2 (Fig. 9*A*). At concentrations exceeding 4 μM AFN-1252, only a single bacterium was detected in each infected cell (Fig. 9*A*). The effect of AFN-1252 on *C. trachomatis* serovar D was also examined to verify that the ability of AFN-1252 to arrest *C. trachomatis* replication was not strain-dependent (Fig. 9*B*). In the D serovar, at AFN-1252 concentrations exceeding 4 μM, only a single bacterium was detected in each infected cell. These data also showed that AFN-1252 prevented the first cell division of *C. trachomatis* following infection. Double staining with Hsp60 (*red*) and a polyclonal antibody against the chlamydial MOMP (*green*) was performed to determine whether EBs differentiated into RBs in AFN-1252-treated cells. EBs were characterized by

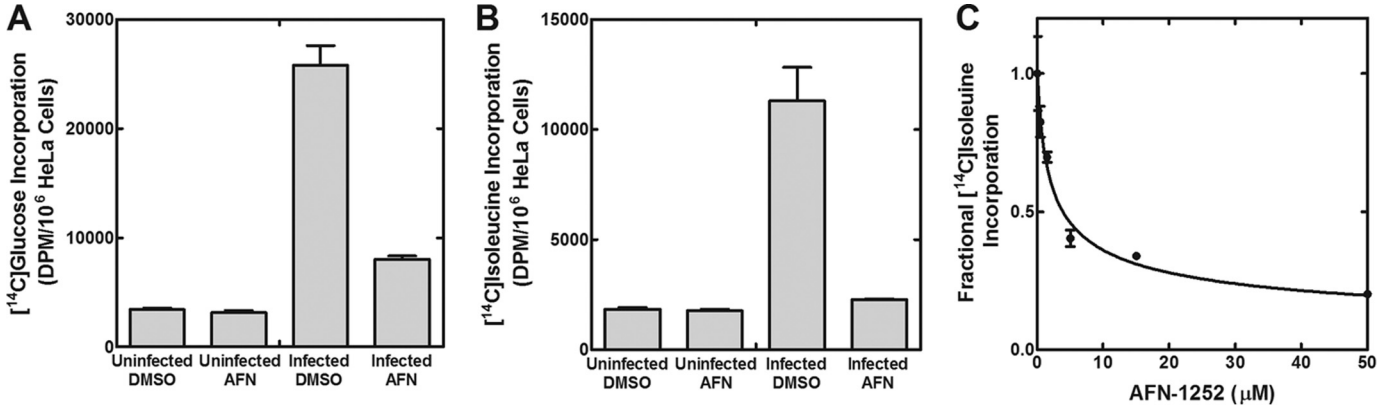

FIGURE 7. **AFN-1252 inhibits *C. trachomatis* FASII.** *A*, [U-^{14}C]glucose incorporation into the lipids of uninfected HeLa cells, uninfected HeLa cells treated with 50 μM AFN-1252, infected HeLa cells, and infected HeLa cells treated with AFN-1252. *B*, [U-^{14}C]isoleucine incorporation into the lipids of uninfected HeLa cells, uninfected HeLa cells treated with AFN-1252, infected HeLa cells, and infected HeLa cells treated with AFN-1252. *C*, [U-^{14}C]isoleucine incorporation into the lipids of infected HeLa cells as a function of increasing concentrations of AFN-1252. HeLa cells were infected at a multiplicity of infection of 5 at time 0. All labeling experiments were conducted by adding AFN-1252 to the cell cultures for 30 min at 20 h postinfection, followed by radioactive pulse labeling for 4 h with the indicated radiochemical. *Error bars*, S.E.

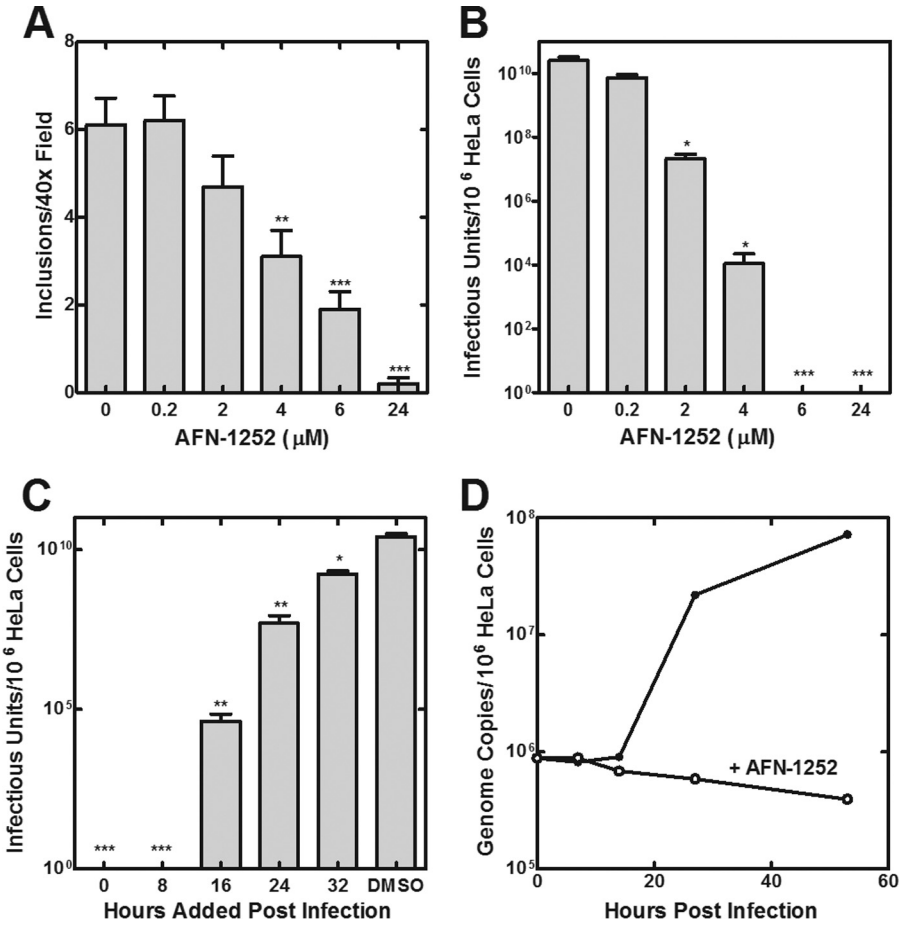

FIGURE 8. **AFN-1252 inhibits *C. trachomatis* replication.** *A*, number of chlamydial inclusions observed per ×40 field at 42 h postinfection was determined as a function of increasing AFN-1252 concentrations added immediately after the infection of HeLa cells with *C. trachomatis* serovar L2. *B*, number of infectious units of *C. trachomatis* serovar L2 generated in the presence of increasing AFN-1252 concentrations added immediately after the initial infection. *C*, number of infectious units of *C. trachomatis* serovar L2 produced when 6 μM AFN-1252 was added at 0, 8, 16, 24, and 32 h after the initiating infection. The number of infectious particles was counted at the end of 48 h in all cases. Six measurements were made in each of two experiments. Significance was determined using Student's *t* test: *, $p < 0.05$; **, $p < 0.01$; ***, $p < 0.001$. *D*, number of *C. trachomatis* serovar L2 genomes during the course of an infection cycle in control and cells treated with 10 μM AFN-1252. *Error bars*, S.E.

a small area of Hsp60 staining completely enclosed by MOMP indicated by a *yellow* cytoplasmic dot surrounded by *green* (Fig. 9*C*). Treatment of *C. trachomatis*-infected cells with rifampicin (RNA synthesis inhibitor) or chloramphenicol (protein synthesis inhibitor) arrested cells in an EB-like state with no change in size or pattern of MOMP or Hsp60 staining compared with EBs (Fig. 9*C*), consistent with RNA and protein synthesis being required to support differentiation into an RB. In the normal

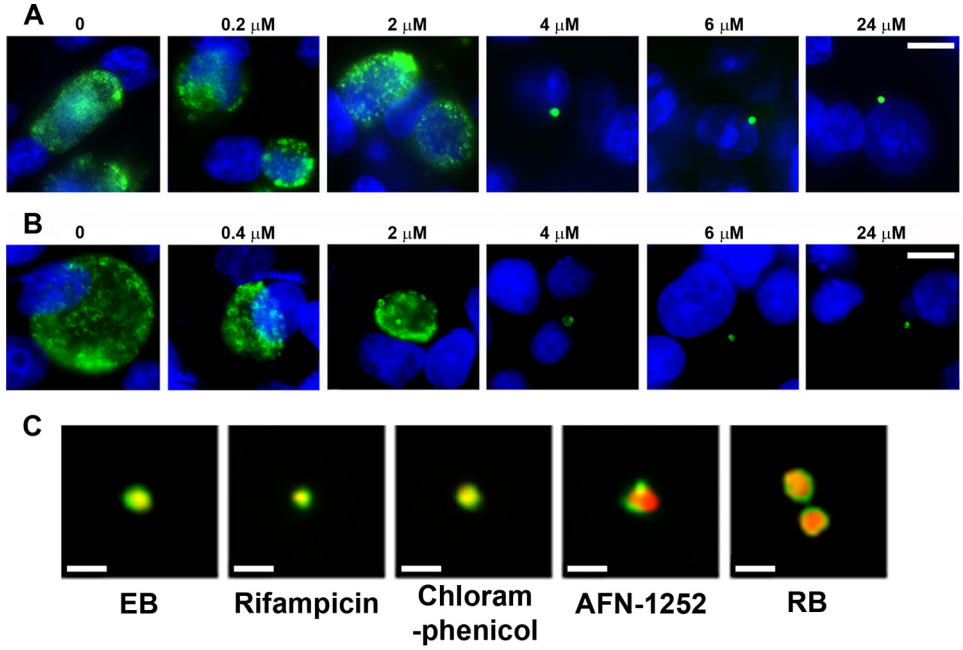

FIGURE 9. **AFN-1252 arrests *C. trachomatis* prior to the first bacterial cell division.** *A*, immunofluorescence staining (antichlamydial Hsp60 antibody in *green* and Hoechst in *blue*) of HeLa cells infected with *C. trachomatis* serovar L2 and treated with increasing concentrations of AFN-1252. *Size bar*, 10 μm. *B*, immunofluorescence staining of HeLa cells infected with *C. trachomatis* serovar D and treated with increasing concentrations of AFN-1252. *Size bar*, 10 μm. *C*, morphology of AFN-1252-treated *C. trachomatis* serovar L2 infection model compared with a typical EB, a typical RB found 6 h after infection, and the appearance of the infection model treated with rifampicin or chloramphenicol at the time of infection. Drug-treated cells were fixed at 24 h postinfection and stained with antibodies directed against MOMP (*green*) and chlamydial Hsp60 (*red*). The EBs were stained at 1 h postinfection, whereas the RB was stained at 14 h postinfection. *Yellow*, overlapping staining. *Size bars*, 0.5 μm.

developmental cycle of *C. trachomatis*, the endocytosed EB differentiates into a slightly larger RB characterized by an expanded, intense cytoplasmic Hsp60 (*red*) staining (Fig. 9*C*). In cells treated with AFN-1252, the internalized bacterium had the characteristics of an RB indicated by an increase in size and the intensity of Hsp60 staining (Fig. 9*C*). The staining of MOMP in AFN-1252-arrested cells was also polarized to one side of the cell. Whether the staining pattern in the presence of AFN-1252 reflected the accumulation of a normal intermediate in the developmental cycle or was due to an effect of the drug is not clear. These data indicated that AFN-1252 arrested *C. trachomatis* after the differentiation into RBs was initiated but before the first bacterial cell division.

DISCUSSION

Our results show that FASII is essential for the replication of *C. trachomatis* within its eukaryotic host. FASII is essential for the synthesis of two major membrane constituents in free-living Gram-negative bacteria. First, FASII supplies the fatty acids required for the synthesis of membrane phospholipids, and second, FASII generates the 3-hydroxy fatty acids required for LOS synthesis. Previous work showed that the selective inhibition of LOS synthesis at the LpxC step permitted the proliferation of *C. trachomatis* within its cytoplasmic inclusion but blocked the terminal differentiation of RBs into EBs (10). If FASII is only required for generating 3-hydroxy fatty acids for LOS synthesis and the bacterium obtains its phospholipids from the host, then AFN-1252 inhibition would have the same effect on the infection cycle as a LOS inhibitor. However, blocking FASII arrests cell replication whenever it is added over the entire developmental cycle, which is consistent with phospholipid synthesis using products derived from FASII as essential for *C. trachomatis* replication. Inhibitors of RNA synthesis (rifampicin) and protein synthesis (chloramphenicol) blocked *C. trachomatis* development at the EB stage, showing that these processes are necessary for EB to RB conversion. *C. trachomatis* had an enlarged, RB-like morphology in AFN-1252-treated cells, indicating that FASII inhibition arrested development after the differentiation from EB to RB is initiated but before the first cell division. The phospholipid classes of *C. trachomatis* reflect the host cell composition (26). Previous work suggests that *C. trachomatis* obtains its phospholipids from the host and modifies a subset of these lipids by introducing a branched-chain fatty acid into the 2-position (3, 26). Additional work is needed to determine whether *C. trachomatis* synthesizes an important class of phospholipids *de novo*, using the products of FASII, or whether the acylation/deacylation pathway is critical for the modification of host phospholipids with branched-chain fatty acids. Nonetheless, it is clear from this study that FASII products are critical for cell division in this parasitic bacterium.

This work identifies FASII, and FabI in particular, as a therapeutic target in *C. trachomatis*. As an intracellular pathogen that acquires vital nutrients from the host, *C. trachomatis* lacks many biochemical pathways that are traditional antibacterial drug targets (44, 45). Although previous work suggested that fatty acids and phospholipids of chlamydial membranes are obtained from the host (45), our study shows that FASII is nonetheless essential for chlamydial replication. AFN-1252 is effective in cell culture against *C. trachomatis* and has pharmacological properties that make it an effective agent against *S. aureus* infections (36, 46). However, its potency may have to

be improved in order for it to be effectively deployed to treat *C. trachomatis*. Our *Ct*FabI·NADH·AFN-1252 crystal structure shows that AFN-1252 inhibits *Ct*FabI by making similar contacts to the backbone amides and nucleotide cofactor as *Sa*FabI (12). Our structure characterization also clearly points to the absence of the Met-99 side chain interaction with the oxotetrahydronaphthyridine ring of AFN-1252 as the primary reason for the lower affinity of AFN-1252 binding to *Ct*FabI compared with *Sa*FabI. This interaction with Met-99 in *Sa*FabI is established to be critical for high-affinity AFN-1252 binding in *Sa*FabI based on the finding that a missense mutation giving rise to a M99T mutation in FabI accounts for acquired resistance to AFN-1252 in *S. aureus* (17). Structure modifications to AFN-1252 that compensate for this interaction should allow for the design of a potent and selective *Ct*FabI inhibitor.

Acknowledgments—We thank Nirun Naher for expert technical assistance and Amanda Nourse (St. Jude Molecular Interaction Analysis Facility) for the analytical ultracentrifugation experiments.

REFERENCES

1. Belland, R., Ojcius, D. M., and Byrne, G. I. (2004) Focus: *Chlamydia*. *Nat. Rev. Microbiol.* **2,** 530–531
2. Becker, Y. (1978) The *Chlamydia*: molecular biology of procaryotic obligate parasites of eucaryocytes. *Microbiol. Rev.* **42,** 274–306
3. Wylie, J. L., Hatch, G. M., and McClarty, G. (1997) Host cell phospholipids are trafficked to and then modified by *Chlamydia trachomatis*. *J. Bacteriol.* **179,** 7233–7242
4. Su, H., McClarty, G., Dong, F., Hatch, G. M., Pan, Z. K., and Zhong, G. (2004) Activation of Raf/MEK/ERK/cPLA$_2$ signaling pathway is essential for chlamydial acquisition of host glycerophospholipids. *J. Biol. Chem.* **279,** 9409–9416
5. Vignola, M. J., Kashatus, D. F., Taylor, G. A., Counter, C. M., and Valdivia, R. H. (2010) cPLA$_2$ regulates the expression of type I interferons and intracellular immunity to *Chlamydia trachomatis*. *J. Biol. Chem.* **285,** 21625–21635
6. Raetz, C. R., Reynolds, C. M., Trent, M. S., and Bishop, R. E. (2007) Lipid A modification systems in Gram-negative bacteria. *Annu. Rev. Biochem.* **76,** 295–329
7. Rund, S., Lindner, B., Brade, H., and Holst, O. (1999) Structural analysis of the lipopolysaccharide from *Chlamydia trachomatis* serotype L2. *J. Biol. Chem.* **274,** 16819–16824
8. Heine, H., Müller-Loennies, S., Brade, L., Lindner, B., and Brade, H. (2003) Endotoxic activity and chemical structure of lipopolysaccharides from *Chlamydia trachomatis* serotypes E and L2 and *Chlamydophila psittaci* 6BC. *Eur. J. Biochem.* **270,** 440–450
9. Heine, H., Gronow, S., Zamyatina, A., Kosma, P., and Brade, H. (2007) Investigation on the agonistic and antagonistic biological activities of synthetic *Chlamydia* lipid A and its use in *in vitro* enzymatic assays. *J. Endotoxin Res.* **13,** 126–132
10. Nguyen, B. D., Cunningham, D., Liang, X., Chen, X., Toone, E. J., Raetz, C. R., Zhou, P., and Valdivia, R. H. (2011) Lipooligosaccharide is required for the generation of infectious elementary bodies in *Chlamydia trachomatis*. *Proc. Natl. Acad. Sci. U.S.A.* **108,** 10284–10289
11. Kaplan, N., Garner, C., and Hafkin, B. (2013) AFN-1252 *in vitro* absorption studies and pharmacokinetics following microdosing in healthy subjects. *Eur. J. Pharm. Sci.* **50,** 440–446
12. Kaplan, N., Albert, M., Awrey, D., Bardouniotis, E., Berman, J., Clarke, T., Dorsey, M., Hafkin, B., Ramnauth, J., Romanov, V., Schmid, M. B., Thalakada, R., Yethon, J., and Pauls, H. W. (2012) Mode of action, *in vitro* activity, and *in vivo* efficacy of AFN-1252, a selective antistaphylococcal FabI inhibitor. *Antimicrob. Agents Chemother.* **56,** 5865–5874
13. Girard, G., Barends, S., Rigali, S., van Rij, E. T., Lugtenberg, B. J. J., and Bloemberg, G. V. (2006) Pip, a novel activator of phenazine biosynthesis in *Pseudomonas chlororaphis* PCL1391. *J. Bacteriol.* **188,** 8283–8293
14. Paoletti, L., Lu, Y.-J., Schujman, G. E., de Mendoza, D., and Rock, C. O. (2007) Coupling of fatty acid and phospholipid synthesis in *Bacillus subtilis*. *J. Bacteriol.* **189,** 5816–5824
15. Pemble, C. W., 4th, Mehta, P. K., Mehra, S., Li, Z., Nourse, A., Lee, R. E., and White, S. W. (2010) Crystal structure of the 6-hydroxymethyl-7,8-dihydropterin pyrophosphokinase·dihydropteroate synthase bifunctional enzyme from *Francisella tularensis*. *PLoS One* **5,** e14165
16. Moldoveanu, T., Grace, C. R., Llambi, F., Nourse, A., Fitzgerald, P., Gehring, K., Kriwacki, R. W., and Green, D. R. (2013) BID-induced structural changes in BAK promote apoptosis. *Nat. Struct. Mol. Biol.* **20,** 589–597
17. Yao, J., Maxwell, J. B., and Rock, C. O. (2013) Resistance to AFN-1252 arises from missense mutations in *Staphylococcus aureus* enoyl-acyl carrier protein reductase (FabI). *J. Biol. Chem.* **288,** 36261–36271
18. Otwinowski, Z., and Minor, W. (1997) Processing of x-ray diffraction data collected in oscillation mode. *Methods Enzymol.* **276,** 307–326
19. McCoy, A. J. (2007) Solving structures of protein complexes by molecular replacement with Phaser. *Acta Crystallogr. D Biol. Crystallogr.* **63,** 32–41
20. Adams, P. D., Afonine, P. V., Bunkóczi, G., Chen, V. B., Echols, N., Headd, J. J., Hung, L. W., Jain, S., Kapral, G. J., Grosse Kunstleve, R. W., McCoy, A. J., Moriarty, N. W., Oeffner, R. D., Read, R. J., Richardson, D. C., Richardson, J. S., Terwilliger, T. C., and Zwart, P. H. (2011) The Phenix software for automated determination of macromolecular structures. *Methods* **55,** 94–106
21. Emsley, P., and Cowtan, K. (2004) Coot: model-building tools for molecular graphics. *Acta Crystallogr. D Biol. Crystallogr.* **60,** 2126–2132
22. DeLano, W. L. (2012) *The PyMOL Molecular Graphics System*, version 1.5.0.1, Schroedinger, LLC, New York
23. Scidmore, M. A. (2005) Cultivation and laboratory maintenance of *Chlamydia trachomatis*. *Curr. Protoc. Microbiol.* Chapter 11, Unit 11A.1
24. Bligh, E. G., and Dyer, W. J. (1959) A rapid method of total lipid extraction and purification. *Can. J. Biochem. Physiol.* **37,** 911–917
25. Kaneda, T. (1991) Iso- and anteiso-fatty acids in bacteria: biosynthesis, function, and taxonomic significance. *Microbiol. Rev.* **55,** 288–302
26. Hatch, G. M., and McClarty, G. (1998) Phospholipid composition of purified *Chlamydia trachomatis* mimics that of the eucaryotic host cell. *Infect. Immun.* **66,** 3727–3735
27. Sweet, C. R., Lin, S., Cotter, R. J., and Raetz, C. R. (2001) A *Chlamydia trachomatis* UDP-*N*-acetylglucosamine acyltransferase selective for myristoyl-acyl carrier protein. Expression in *Escherichia coli* and formation of hybrid lipid A species. *J. Biol. Chem.* **276,** 19565–19574
28. Kosma, P. (1999) Chlamydial lipopolysaccharide. *Biochim. Biophys. Acta* **1455,** 387–402
29. Qureshi, N., Kaltashov, I., Walker, K., Doroshenko, V., Cotter, R. J., Takayama, K., Sievert, T. R., Rice, P. A., Lin, J. S., and Golenbock, D. T. (1997) Structure of the monophosphoryl lipid A moiety obtained from the lipopolysaccharide of *Chlamydia trachomatis*. *J. Biol. Chem.* **272,** 10594–10600
30. Heath, R. J., and Rock, C. O. (1995) Enoyl-acyl carrier protein reductase (*fabI*) plays a determinant role in completing cycles of fatty acid elongation in *Escherichia coli*. *J. Biol. Chem.* **270,** 26538–26542
31. Heath, R. J., and Rock, C. O. (1996) Regulation of fatty acid elongation and initiation by acyl-acyl carrier protein in *Escherichia coli*. *J. Biol. Chem.* **271,** 1833–1836
32. Bergler, H., Högenauer, G., and Turnowsky, F. (1992) Sequences of the *envM* gene and two mutated alleles in *Escherichia coli*. *J. Gen. Microbiol.* **138,** 2093–2100
33. White, S. W., Zheng, J., Zhang, Y.-M., and Rock, C. O. (2005) The structural biology of type II fatty acid biosynthesis. *Annu. Rev. Biochem.* **74,** 791–831
34. Schiebel, J., Chang, A., Lu, H., Baxter, M. V., Tonge, P. J., and Kisker, C. (2012) *Staphylococcus aureus* FabI: inhibition, substrate recognition, and potential implications for *in vivo* essentiality. *Structure* **20,** 802–813
35. Xu, H., Sullivan, T. J., Sekiguchi, J., Kirikae, T., Ojima, I., Stratton, C. F., Mao, W., Rock, F. L., Alley, M. R., Johnson, F., Walker, S. G., and Tonge, P. J. (2008) Mechanism and inhibition of saFabI, the enoyl reductase from *Staphylococcus aureus*. *Biochemistry* **47,** 4228–4236
36. Banevicius, M. A., Kaplan, N., Hafkin, B., and Nicolau, D. P. (2013) Phar-

macokinetics, pharmacodynamics, and efficacy of novel FabI inhibitor AFN-1252 against MSSA and MRSA in the murine thigh infection model. *J. Chemother.* **25,** 26–31
37. Rozwarski, D. A., Vilchèze, C., Sugantino, M., Bittman, R., and Sacchettini, J. C. (1999) Crystal structure of the *Mycobacterium tuberculosis* enoyl-ACP reductase, InhA, in complex with NAD^+ and a C16 fatty acyl substrate. *J. Biol. Chem.* **274,** 15582–15589
38. Rafi, S., Novichenok, P., Kolappan, S., Zhang, X., Stratton, C. F., Rawat, R., Kisker, C., Simmerling, C., and Tonge, P. J. (2006) Structure of acyl carrier protein bound to FabI, the FASII enoyl reductase from *Escherichia coli*. *J. Biol. Chem.* **281,** 39285–39293
39. Suh, M. C., Schultz, D. J., and Ohlrogge, J. B. (1999) Isoforms of acyl carrier protein involved in seed-specific fatty acid synthesis. *Plant J.* **17,** 679–688
40. Priyadarshi, A., Kim, E. E., and Hwang, K. Y. (2010) Structural insights into *Staphylococcus aureus* enoyl-ACP reductase (FabI), in complex with NADP and triclosan. *Proteins* **78,** 480–486
41. Qiu, X., Janson, C. A., Court RI, Smyth, M. G., Payne, D. J., and Abdel-Meguid, S. S. (1999) Molecular basis for triclosan activity involves a flipping loop in the active site. *Protein Sci.* **8,** 2529–2532
42. Rock, C. O., and Jackowski, S. (2002) Forty years of fatty acid biosynthesis. *Biochem. Biophys. Res. Commun.* **292,** 1155–1166
43. Hutson, S. M., Sweatt, A. J., and Lanoue, K. F. (2005) Branched-chain amino acid metabolism: implications for establishing safe intakes. *J. Nutr.* **135,** 1557S–1564S
44. Stephens, R. S., Kalman, S., Lammel, C., Fan, J., Marathe, R., Aravind, L., Mitchell, W., Olinger, L., Tatusov, R. L., Zhao, Q., Koonin, E. V., and Davis, R. W. (1998) Genome sequence of an obligate intracellular pathogen of humans: *Chlamydia trachomatis*. *Science* **282,** 754–759
45. Saka, H. A., and Valdivia, R. H. (2010) Acquisition of nutrients by Chlamydiae: unique challenges of living in an intracellular compartment. *Curr. Opin. Microbiol.* **13,** 4–10
46. Parsons, J. B., Kukula, M., Jackson, P., Pulse, M., Simecka, J. W., Valtierra, D., Weiss, W. J., Kaplan, N., and Rock, C. O. (2013) Perturbation of *Staphylococcus aureus* gene expression by the enoyl-acyl carrier protein reductase inhibitor AFN-1252. *Antimicrob. Agents Chemother.* **57,** 2182–2190
47. Braberg, H., Webb, B. M., Tjioe, E., Pieper, U., Sali, A., and Madhusudhan, M. S. (2012) SALIGN: a web server for alignment of multiple protein sequences and structures. *Bioinformatics* **28,** 2072–2073
48. Gouet, P., Courcelle, E., Stuart, D. I., and Métoz, F. (1999) ESPript: analysis of multiple sequence alignments in PostScript. *Bioinformatics* **15,** 305–308